Imaging Freeze-Out Sources and Extracting Strong Interaction Parameters in Relativistic Heavy-Ion Collisions

Junhuai Xu(许俊怀)[1], Zhi Qin(秦智)[1*], Renjie Zou(邹仁杰)[1], Dawei Si(司大伟)[1], Sheng Xiao(肖圣)[1], Baiting Tian(田柏汀)[1], Yijie Wang(王轶杰)[1*], and Zhigang Xiao(肖志刚)[1,2*]

[1]*Department of Physics, Tsinghua University, Beijing 100084, China*
[2]*Center of High Energy Physics, Tsinghua University, Beijing 100084, China*

(Received 18 February 2025; accepted manuscript online 25 February 2025)

By combining femtoscopic interferometry with an optical deblurring algorithm, we present a novel method to image the source in heavy-ion collisions (HICs), while simultaneously determining the interaction strength between particle pairs. The spatial distribution of the emission source has been reconstructed for protons (p) and antiprotons ($\bar{p}$) from the respective pp and $\bar{p}\bar{p}$ correlation functions in Au+Au collisions at $\sqrt{S_{\rm NN}} = 200$ GeV. Within experimental uncertainties, protons and antiprotons share the same freeze-out distribution showing higher density in the center compared to the widely assumed Gaussian shape. The results evidence the matter–antimatter symmetry in coordinate space at the freeze-out moment before the nucleons are fully randomized in the collisions.

DOI: 10.1088/0256-307X/42/3/031401 CSTR: 32039.14.0256-307X.42.3.031401

Introduction. It is well established that matter and antimatter were created in equal amounts during the first moments after the Big Bang. However, the observable universe consists overwhelmingly of matter, posing a fundamental question in physics. This puzzling phenomenon is related to the profound symmetry breaking in nature and remains a challenge in nuclear and particle physics. On modern accelerators, heavy-ion collisions (HICs) create conditions akin to those in the early universe. So after the success of observing the production of antimatter,[1–3] researchers can further investigate the spatial evolution and decoupling of the matter and antimatter on the femtoscopic scale.

Hanbury Brown and Twiss (HBT) intensity interferometry, originally developed to measure the angular radius of Sirius,[4] has been extensively adapted in nuclear physics.[5–7] It enables the extraction of spatiotemporal characteristics of the emission source in HICs by analyzing particle-pair correlation functions (CFs) at small relative momenta.[8,9] Additionally, the spatial information embedded in the CFs has been applied to investigate the exotic structure and rare decay mode of unstable nuclei.[10–14] In a basic picture, the CF is the result of the low-energy scattering between the particle pair emitted from the source. It carries the information of the interaction strength, defined by the scattering length f_0 and effective range d_0 between the pair, written as (f_0, d_0) in short.

Thus, simultaneous inference of the source distribution and the interaction strength becomes feasible for either particle or antiparticle pairs. Based on the Lednický–Lyuboshitz (LL) model, STAR collaboration has verified that protons and antiprotons exhibit nearly identical interaction properties, and the extracted source size parameters for pp and $\bar{p}\bar{p}$ pairs were found to be similar.[15] Specifically, within experimental uncertainties, the parameters (f_0, d_0) are equivalent for pp and $\bar{p}\bar{p}$ pairs, consistent with CPT symmetry, a fundamental principle in physical laws. The Gaussian source assumption has become widely adopted in correlation function analysis, from which significant results have been obtained in the studies of particle interactions and source distributions.[16–19]

However, more studies start to notice the non-Gaussian feature of the source. By Gaussian parameterization, it is assumed that all the participants are totally randomized in space prior to the freeze-out instant, and the initial state as well as the evolution details of the colliding system are lost. This strong assumption is unfavorable in the context of various recent studies. For two examples, i) high energy HIC has been applied to infer the initial shape of the colliding nuclei;[20,21] ii) Ohm's law is suggestively broken because of the strong field and extremely short evolution time.[22] In both cases, it is of importance to probe the spatial evolution of the colliding system. In recent experiments, a similar deviation from Gaussian distributions has been observed in the freeze-out source distributions of particles, exhibiting long tails and Lévy stable characteristics.[23–28] This behavior suggests that hadronic evolution could be described by Lévy walks, where the movement patterns are governed by long-tailed random walks. This concept has already played a significant role in the natural sciences,[29,30] and is gradually gaining widespread attention in the field of heavy-ion collisions. Thus, it is crucial to obtain the true distribution without pre-assuming a specific form such as the Gaussian.

Despite the difficulty in solving inverse problem, the

*Corresponding author. Email: qinz18@mails.tsinghua.edu.cn; yj-wang15@tsinghua.org.cn; xiaozg@tsinghua.edu.cn
© 2025 Chinese Physical Society and IOP Publishing Ltd. All rights, including for text and data mining, AI training, and similar technologies, are reserved.

direct imaging of the source has been achieved without introducing the analytic parameterization.[31–33] More recently, the Bayesian-based deblurring method, known as Richardson-Lucy (RL) algorithm[34,35] which was initially developed for optical imaging,[36,37] has gained prominence in nuclear physics.[38–42] Particularly, the RL algorithm has been applied in source imaging in HICs, highlighting the method's effectiveness and robustness.[39,43] In this Letter, combining the RL deblurring algorithm and the LL model incorporating the pair interaction, we realize the solution to the inverse problem of source imaging from the experimental CFs. The source distribution and (f_0, d_0) are determined simultaneously. The similarity of the source spatial distribution of p and $\bar{p}$ emission has been demonstrated.

Methodology. Defined as a function of the relative momentum $\boldsymbol{q} = \boldsymbol{p}_1 - \boldsymbol{p}_2$ in the particle pair rest frame (PRF), the CF is given experimentally by $C(\boldsymbol{q}) = \frac{P(\boldsymbol{p}_1, \boldsymbol{p}_2)}{P(\boldsymbol{p}_1)P(\boldsymbol{p}_2)}$, where $P(\boldsymbol{p}_1)$ and $P(\boldsymbol{p}_2)$ are the probabilities of detecting particles with momenta $\boldsymbol{p}_1$ and $\boldsymbol{p}_2$, respectively, and $P(\boldsymbol{p}_1, \boldsymbol{p}_2)$ is the joint probability of detecting both particles simultaneously. For uncorrelated emissions, $C = 1$ is expected. In theoretical frameworks, the correlation function (CF) is computed using the Koonin-Pratt (KP) formula[44,45]

$$C(\boldsymbol{q}) = \int d^3r |\Psi_{\boldsymbol{q}}(\boldsymbol{r}')|^2 S(\boldsymbol{r}), \tag{1}$$

where S is the source function (SF) related to the relative distance $\boldsymbol{r} = \boldsymbol{r}_1 - \boldsymbol{r}_2$ of the particle-pair in the source rest frame, and $\Psi_{\boldsymbol{q}}(\boldsymbol{r}')$ is the wave function calculated from the relative momentum $\boldsymbol{q}$ and distance $\boldsymbol{r}'$ in the PRF. Based on the LL model,[46] the interaction strength between particle pair is characterized by (f_0, d_0) describing the strong interaction scattering amplitude in S-wave expansion under the effective range approximation.

In optical deblurring, the measured distribution ($f(\nu)$) is related to the true photon distribution ($\mathcal{F}(\mu)$) through a conditional probability function ($P(\nu|\mu)$),

$$f(\nu) = \int P(\nu|\mu)\mathcal{F}(\mu)d\mu, \tag{2}$$

where the response function $P(\nu|\mu)$ represents the conditional probability that a photon with the true property μ is measured as ν. Although the true distribution $\mathcal{F}(\mu)$ is unknown, it can be inferred from the measured distribution $f(\nu)$ through iterative regression starting from an arbitrary initial guess. This iterative process is illustrated in Fig. 1. Starting with $t = 0$, the arbitrary initial trial $\mathcal{F}^{(0)}(\mu)$ is convolved with $P(\nu|\mu)$ to predict the measurement distribution $f^P(\nu)$, which is then compared to the known measurement distribution $f(\nu)$. Based on the difference between them, an amplification factor $A^{(t)}$ is calculated at each t^{th} iteration. The factor $A^{(t)}$ is functioning to adjust the values of $\mathcal{F}^{(t)}(\mu)$ for the next iteration. Through the iterative process, the updated distribution

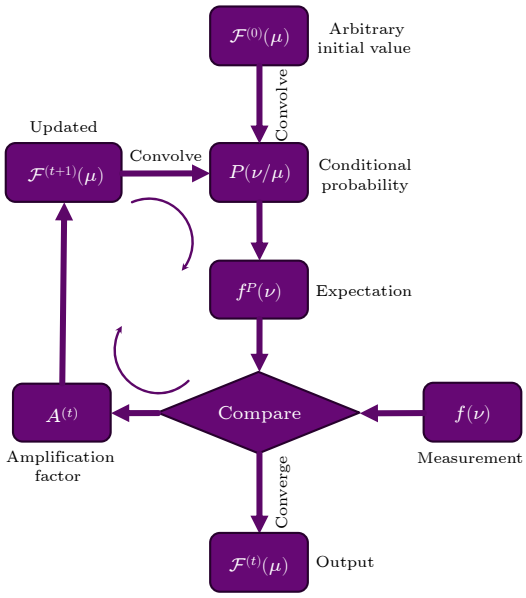

Fig. 1. Diagram of RL algorithm process.

$\mathcal{F}^{(t+1)}(\mu)$ progressively converges toward the true distribution $\mathcal{F}(\mu)$. The convergence criteria is invoked if $f^P(\nu)$ becomes sufficiently close to $f(\nu)$.

From the mathematical similarity between the KP formula (1) and the optical deblurring equation (2), it is naturally suggested that the RL algorithm can be applied iteratively to solve the SF. By evaluating the converged χ^2 value, one can identify the optimal (f_0, d_0) for the wave function that best describes the CF, thereby achieving both SF imaging and extraction of the strong interaction parameters simultaneously. For the convenience of numerical implementation, the KP formula is discretized by dividing C into N bins and S into M bins ($N \geq M$). After discretization, the RL algorithm is used to iteratively solve for the distribution of the source function.[39,42] The CF C is expressed by S through an $N \times M$ transformation matrix K as $C_i = \sum_{j=1}^{M} K_{ij} S_j$. This transformation matrix is calculated by

$$K_{ij} = \int_{\text{bin}_j} d\boldsymbol{Q} |\Psi_{\boldsymbol{q}_i}(\boldsymbol{r}')|^2 r^2 \sin\theta dr d\theta d\varphi, \tag{3}$$

where $\boldsymbol{Q}$ denotes the total momentum of the particle pair in the source rest frame. Here, i and j label the bin indices of C and S, respectively. In one-dimensional imaging, the wave function is assumed to be uniform in the polar θ and azimuthal φ directions, only leaving the r-direction to consider. Consequently, the integration over θ and φ can be performed using Monte Carlo sampling uniformly within the spherical shell. This approach allows for iterative reconstruction of the source distribution from the discretized experimental measurements of C.

Model Test. The imaging of the source and the extraction of interaction parameters (f_0, d_0) can now be achieved simultaneously using this method. To test the algorithm, we start with calculating the CF from the given source distribution and known pp interactions with $f_0 = 7.8\,\text{fm}$ and $d_0 = 2.77\,\text{fm}$. In order to mimic the real measurement, we introduce fluctuations to each point according to the

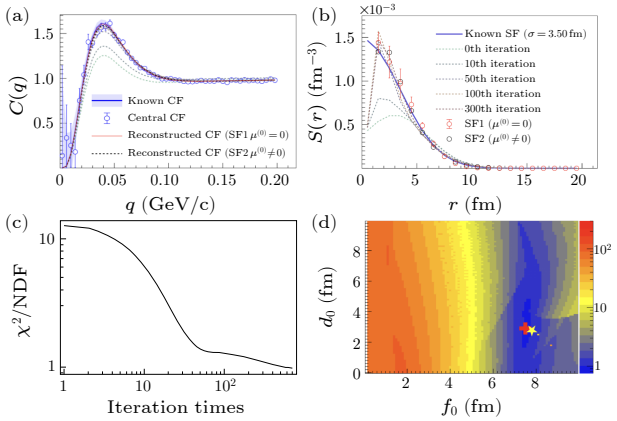

Fig. 2. Model test procedure. (a) The correlations functions. The blue solid curve is the CF calculated using LL model. The symbols are the sampled CF taking into account the uncertainty to mimic the experimental measurement which is selected as the central CF for imaging. The dashed curves are the output at various iteration steps. The red solid and black dashed thin curves are the final reconstructed CF with two different initial trials of the source function SF1 and SF2. (b) The restored source images. The blue solid curve is the given SF to calculate the CF. The red and black symbols are the restored SF at two initial trials SF1 and SF2. (c) The χ^2/NDF as a function of iteration times. (d) The minimum χ^2/NDF on the (f_0, d_0) plane. The yellow star and red cross denote the input value and the final converged solution.

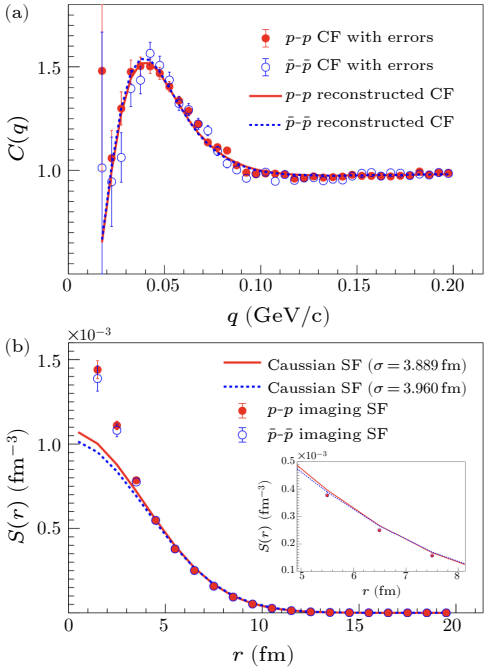

Fig. 3. (a) Reconstructed correlation functions (CFs) for pp (red solid curve) and $\bar{p}\bar{p}$ (blue dashed curve) pairs, compared with experimental data from Ref. [15] (red dots for pp and blue circles for $\bar{p}\bar{p}$ pairs). (b) Reconstructed SFs for p (red dots) and $\bar{p}$ (blue circles) in Au+Au at the center of mass energy of 200 GeV. The symbols are the results of direct imaging without Gaussian assumption. The SFs with Gaussian shape obtained in Ref. [15] are shown by the curves for reference.

experimental uncertainty. Figure 2(a) shows the theoretic CF (thick solid curve) and the fluctuated CF (open circle). Then, the inverse problem is iteratively solved from an initial trial of the SF, which is taken as a Gaussian distribution with $\mu = 0$ center location and arbitrary deviation. The reconstructed SF ends close to the known one, marked as SF1 in Fig. 2(b). In order to check the robustness of the algorithm against the variation of the initial SF, we also test the second initial trial, where the center of the initial Gaussian is arbitrarily set at $\mu = 3$ fm instead of zero peaking. As the iteration progresses, the output SF gradually converges to the known one, as illustrated by the dashed curves in Fig. 2(b). The marked SF2 sits on the top of SF1, evidencing the robustness of the iterative procedure. Figure 2(c) presents the closeness quantity χ^2 over iteration times in the imaging process of the central CF. Here χ^2 is defined as $\chi^2 = \sum_i^N (\frac{C_i^P - C_i}{\sigma_i})^2$, where C_i^P represents the value of the i^{th} point. During the procedure, (f_0, d_0) parameters are optimized by minimum χ^2 and the closeness between the output and the known CF is checked in every iteration till the convergence condition is reached, namely, the change of χ^2 between two successive iterations is less than 1×10^{-4}, which functions as a threshold to avoid noise amplification. Figure 2(d) shows the minimum χ^2 distribution on the (f_0, d_0) plane. The optimized (f_0, d_0), marked by red cross, converge to the input one (yellow star). The consistency between the input values and the reconstructed ones in panels (a), (b), and (d) demonstrates the validity of the deblurring algorithm.

Application to Data. Now we apply the method to the pp and $\bar{p}\bar{p}$ CFs in Au+Au at $\sqrt{S_{\rm NN}} = 200$ GeV,[47] taken by STAR collaboration[15,48] at the Relativistic Heavy Ion Collider (RHIC).[49,50] The experimental CFs are inclusive and contain the contributions from the residual CFs of $p\Lambda$ and $\Lambda\Lambda$. The residual contribution, which shall be subtracted, is derived by the difference between the two fitting curves with and without the feedback corrections shown in Ref. [47]. The pure pp and $\bar{p}\bar{p}$ CFs are presented in Fig. 3(a) by the symbols, where the uncertainties are the same as in the experiment for each data point.

In the calculation of the Kernel K_{ij}, one needs the momentum distribution of p and $\bar{p}$. The transverse momentum $p_{\rm t}$ distributions are taken from the midrapidity range in the same colliding system[51] measured by PHENIX experiment.[52,53] The longitudinal rapidity $y_{\rm l}$ as well as the azimuth in transverse direction are uniformly distributed. The cuts $0.4 < p_{\rm t} < 2.5$ GeV/c and $|y_{\rm l}| < 0.7$ are the same as STAR data, where the CFs are measured. It is well established that the LL model exhibits limited sensitivity to the parameter d_0 when applied to experimental data analysis. The variation of d_0 brings corresponding uncertainty to the source function to be extracted. Hence, the widely accepted theoretical and experimental approximation $d_0 = 2.8$ fm is fixed here for both pp and $\bar{p}\bar{p}$ pairs. The convergence criterion is set to 1×10^{-2}. The corresponding optimal values of obtained f_0 are as follows:

$$f_{0(pp)} = (7.7 \pm 0.2)\ \text{fm}, \quad f_{0(\bar{p}\bar{p})} = (7.9 \pm 0.3)\ \text{fm}. \tag{4}$$

The f_0 values for pp and $\bar{p}\bar{p}$ pairs are identical and consistent with both the theoretical calculations and the experimental results from STAR collaboration.[15]

The converged CFs of pp and $\bar{p}\bar{p}$ pairs exhibit excellent agreement with the experimental data, as demonstrated by the solid and dashed curves in Fig. 3(a), respectively. The results of the restored source imaging are plotted in panel (b) by red dots for p and blue circles for $\bar{p}$. In order to estimate the uncertainty of each imaging point, numerous pseudo-CFs for pp and $\bar{p}\bar{p}$ are sampled, smearing the content in each individual q bin by Gaussian fluctuation, for which the center (standard deviation) is taken from the experimental value (uncertainty). Then, the standard deviation of the reconstructed SFs are calculated and plotted on each data point bin-by-bin as the error bar on the SF.

The direct imaging result in Fig. 3(b) has important implications. First, within the uncertainty, protons and antiprotons share the identical source distribution at the freeze-out instant. In addition to the momentum distribution analysis conducted in Ref. [47], the direct imaging results presented here provide the final piece of evidence supporting matter–antimatter symmetry in coordinate space, as it pertains to their production and evolution in high-energy HICs. Notably, this evidence is obtained without imposing any assumptions regarding the shape of the source. Second, the profile of the reconstructed SFs deviates from the Gaussian distribution for both protons and antiprotons. Quantitative calculation yields the probability for the SF to be Gaussian is 0 and 2.2×10^{-14} for p and $\bar{p}$, respectively. For a clear comparison, the Gaussian distribution obtained in Ref. [47] are shown by the curves in panel (b), respectively. The emission source is more concentrated at smaller radii ($r < 5\,\mathrm{fm}$), while showing reduced density at larger radii ($5 < r < 8\,\mathrm{fm}$), as highlighted in the inset. It is consistent with the picture of an extremely fast collision. Namely, protons and antiprotons, formed by the coalescence of quarks and antiquarks created inside the overlapping region, are not fully randomized in coordinate space prior to the freeze-out instant. Otherwise, they are expected to extend to the outer space in Gaussian distribution as a deduction of the central limit theorem. Our work offers a support to the recent idea of probing the initial shape and fluctuation of the nucleus via relativistic HIC,[21,54–61] since the collision is so rapid that the spatial information of the colliding nuclei is partially preserved.

The impact of the bin-by-bin variation of the SF on the CF has been analyzed. It is observed that variations in the first few bins of the source function (except for the first bin which is below the low limit cut in LL model calculation) significantly impact the CF, whereas the variations at larger r values are less influential. Inversely, the experimental uncertainty of the CFs near the peak ($q \approx 40\,\mathrm{MeV}$) brings considerable variation to the SF. In order to achieve more accurate imaging, it is demanded to further reduce the uncertainty of the CF, particularly at small q.

The method developed in this work holds significant potential for important applications. Given high-precision experimental CFs, this technique provides a novel approach to identify exotic nuclear structures, particularly in future radioactive ion beam facilities. For instance, it could be employed to probe the proton density profile of bubble nuclei—a recently proposed phenomenon[62,63] that remains under debate.[64] Furthermore, when extended to three dimensions, this method could be applied at facilities such as RHIC to investigate higher-order deformations of atomic nuclei, which are typically studied through nuclear spectroscopy.[65,66]

Summary. A direct imaging method on the femtometer scale has been realized by combining the Richardson-Lucy deblurring algorithm and the intensity interferometry in relativistic heavy-ion collisions. This method allows for a more accurate extraction of source distributions and the final state interactions between particle pair based on the Lednický–Lyuboshitz model analysis. Applying this imaging method to pp and $\bar{p}\bar{p}$ correlation functions in Au+Au at $\sqrt{S_{\mathrm{NN}}} = 200\,\mathrm{GeV}$ measured by the STAR collaboration, we observe the same freeze-out source functions for p and $\bar{p}$ emissions with distinct non-Gaussian characteristics. These findings confirm the matter–antimatter symmetry in coordinate space once produced and suggest the ultrafast feature of the evolution of the collision, which is hardly accessible through other experimental means alone. This method can be extended to three-dimensional imaging for further applications and is inherently compatible with machine-learning approaches,[67] opening new avenues for high-precision source reconstruction in heavy-ion collisions. It represents a significant advancement of our ability to image the femtoscopic heavy-ion collisions and to explore the matter–antimatter physics in terrestrial laboratories.

Acknowledgements. This work is supported by the National Natural Science Foundation of China (Grant Nos. 12335008 and 12205160). The authors acknowledge the support of the Center for High Performance Computing and Initiative Scientific Research Program in Tsinghua University. Sincere gratitude is extended to Nu Xu and Pengfei Zhuang for their valuable suggestions and insightful discussions.

References

[1] Abelev B I, Abelev B I, Aggarwal M M *et al.* (STAR) 2010 *Science* **328** 58
[2] Agakishiev H, Aggarwal M M, Ahammed Z *et al.* (STAR) 2011 *Nature* **473** 353
[3] Abdulhamid M I, Aboona B E, Adam J *et al.* (STAR) 2024 *Nature* **632** 1026
[4] Brown R H and Twiss R Q 1956 *Nature* **178** 1046
[5] Wang Y J, Guan F H, Wu Q H *et al.* 2022 *Phys. Lett. B* **825** 136856
[6] Wang Y J, Guan F H, Diao X Y *et al.* 2021 *Nucl. Sci. Tech.* **32** 4
[7] Qiao F H, Deng X G, and Ma Y G 2024 *Phys. Lett. B* **850** 138535

[8] Wang T T, Ma Y G, and Zhang S 2024 *Phys. Rev. C* **109** 024912
[9] Wang T T, Ma Y G, and Zhang S 2023 *Phys. Rev. C* **107** 014911
[10] Zhou L, Fang D Q, Wang S M, and Hua H 2024 *Nuclear Science and Techniques* **35** 107
[11] Revel A, Marqués F M, Sorlin O *et al.* (R3B) 2018 *Phys. Rev. Lett.* **120** 152504
[12] Laurent B, Marqués F M, Angulo C *et al.* 2019 *J. Phys. G* **46** 03LT02
[13] Cao X G, Cai X Z, Ma Y G, Fang D Q, Zhang G Q, Guo W, Chen J G and Wang J S 2012 *Phys. Rev. C* **86** 044620
[14] Zhou L, Wang S M, Fang D Q and Ma Y G 2022 *Nucl. Sci. Tech.* **33** 105
[15] Adamczyk L, Adkins J K, Agakishiev G *et al.* (STAR) 2015 *Nature* **527** 345
[16] Goldhaber G, Goldhaber S, Lee W Y and Pais A 1960 *Phys. Rev.* **120** 300
[17] Boal D H and Shillcock J C 1986 *Phys. Rev. C* **33** 549
[18] Boal D H, Gelbke C K and Jennings B K 1990 *Rev. Mod. Phys.* **62** 553
[19] Verde G, Brown D A, Danielewicz P, Gelbke C K, Lynch W G and Tsang M B 2002 *Phys. Rev. C* **65** 054609
[20] Abdulhamid M I *et al.* (STAR collaboration) 2024 *Nature* **635** 67
[21] Zhao S J, Xu H J, Zhou Y, Liu Y X, and Song H C 2024 *Phys. Rev. Lett.* **133** 192301
[22] Wang Z Y, Zhao J X, Greiner C, Xu Z, and Zhuang P F 2022 *Phys. Rev. C* **105** L041901
[23] Adare A, Aidala C, Ajitanand N N *et al.* (PHENIX) 2018 *Phys. Rev. C* **97** 064911
[24] Mukherjee A 2023 *Universe* **9** 300
[25] Kovács L 2023 *Universe* **9** 336
[26] Kincses D (STAR) 2024 *Universe* **10** 102
[27] Abdulameer N J, Acharya U, Adare A *et al.* (PHENIX) 2024 *Phys. Rev. C* **110** 064909
[28] Kincses D, Nagy M, and Csanád M 2025 *Commun. Phys.* **8** 55
[29] Tsallis C, Levy S V F, Souza A M C and Maynard R 1995 *Phys. Rev. Lett.* **75** 3589
[30] Zaburdaev V, Denisov S and Klafter J 2015 *Rev. Mod. Phys.* **87** 483
[31] Brown D A and Danielewicz P 1997 *Phys. Lett. B* **398** 252
[32] Chung P, Ajitanand N N, Alexander J M *et al.* 2003 *Phys. Rev. Lett.* **91** 162301
[33] Brown D A, Enokizono A, Heffner M, Soltz R, Danielewicz P and Pratt S 2005 *Phys. Rev. C* **72** 054902
[34] Richardson W H 1972 *J. Opt. Soc. Am.* **62** 55
[35] Lucy L B 1974 *Astron. J.* **79** 745
[36] Vankawala F, Ganatra A, and Patel A 2015 *International Journal of Computer Applications* **116** 15
[37] Liu Y M, Panezai S, Wang Y T, and Stallinga S 2025 *Nature Communications* **16** 911
[38] Danielewicz P and Kurata-Nishimura M 2022 *Phys. Rev. C* **105** 034608
[39] Nzabahimana P and Danielewicz P 2023 *Phys. Lett. B* **846** 138247
[40] Nzabahimana P, Redpath T, Baumann T, Danielewicz P, Giuliani P, and Guèye P 2023 *Phys. Rev. C* **107** 064315
[41] Vargas J, Benlliure J, and Caamaño M 2013 *Nuclear Instruments and Methods in Physics Research Section A* **707** 16
[42] Xu J H, Qin Y H, Qin Z, Si D W, Zhang B Y, Wang Y J, Niu Q L, Xu C, and Xiao Z G 2024 *Phys. Lett. B* **857** 139009
[43] Tam C K, Chajecki Z, Danielewicz P and Nzabahimana P 2025 arXiv:2502.09478 [nucl-th]
[44] Koonin S E 1977 *Phys. Lett. B* **70** 43
[45] Pratt S, Csörgő T, and Zimányi J 1990 *Phys. Rev. C* **42** 2646
[46] Lednicky R and Lyuboshits V L 1981 *Yad. Fiz.* **35** 1316
[47] Zhang Z Q and Ma Y G 2017 *Nucl. Phys. Rev.* **34** 296
[48] Ackermann K H, Adams N, Adler C *et al.* (STAR) 2003 *Nucl. Instrum. Meth. A* **499** 624
[49] Harrison M, Ludlam T and Ozaki S 2003 *Nucl. Instrum. Meth. A* **499** 235
[50] STAR collaboration 2016 *HEPData*
[51] PHENIX Collaboration 2022 *HEPData*
[52] Adler S S, Afanasiev S, Aidala C *et al.* (PHENIX) 2004 *Phys. Rev. C* **69** 034909
[53] Adcox K, Adler S S, Aizama M *et al.* (PHENIX) 2003 *Nucl. Instrum. Meth. A* **499** 469
[54] Jia J, Giacalone G and Zhang C 2023 *Phys. Rev. Lett.* **131** 022301
[55] Zhang C and Jia J 2022 *Phys. Rev. Lett.* **128** 022301
[56] Jia J 2022 *Phys. Rev. C* **105** 014905
[57] Giacalone G, Jia J and Zhang C 2021 *Phys. Rev. Lett.* **127** 242301
[58] Liu Q, Zhao S, Xu H J and Song H 2024 *Phys. Rev. C* **109** 034912
[59] Jia J, Giacalone G, Bally B *et al.* 2024 *Nucl. Sci. Tech.* **35** 220
[60] Schenke B 2024 *Nuclear Science and Techniques* **35** 115
[61] Wang J F, Xu H J and Wang F Q 2024 *Nuclear Science and Techniques* **35** 108
[62] Mutschler A, Lemasson A, Sorlin O *et al.* 2017 *Nature Phys.* **13** 152
[63] Natowitz J B 2024 *Nuclear Science and Techniques* **35** 187
[64] Chen J, Kay B P, Hoffman C R *et al.* 2024 *Phys. Lett. B* **853** 138678
[65] Frauendorf S 2024 *Nucl. Sci. Tech.* **35** 123
[66] Wei K, Ye Y L and Yang Z H 2024 *Nuclear Science and Techniques* **35** 216
[67] Wang L and Zhao J 2024 arXiv:2411.16343 [nucl-th]